Appl. Phys. B 79, 603–609 (2004)
DOI: 10.1007/s00340-004-1592-5

Applied Physics B
Lasers and Optics

E. GIORGETTI[1,✉]
G. MARGHERI[2]
T. DELROSSO[2]
S. SOTTINI[1]
M. MUNIZ-MIRANDA[3]
M. INNOCENTI[3]

A study of the degradation of poly(3-octylthiophene)-based light emitting diodes by Surface Enhanced Raman Scattering

[1] INSTM e Istituto di Fisica Applicata "Nello Carrara"– CNR, Via Panciatichi 64, 50127 Firenze, Italy
[2] Istituto di Fisica Applicata "Nello Carrara"– CNR, Via Panciatichi 64, 50127 Firenze, Italy
[3] Dipartimento di Chimica, Università di Firenze, Via della Lastruccia 3, 50019, Sesto Fiorentino, Italy

Received: 5 April 2004/Revised version: 7 June 2004
Published online: 11 August 2004 •

ABSTRACT Organic light emitting diodes (OLED) based on poly(3-octylthiophene) (P3OT) were studied by on-line Surface Enhanced Raman Scattering (SERS) experiments. A simultaneous reduction of the emitted power and an increase of the SERS signal was observed above an 8 V bias voltage in the case of ITO/P3OT/Al structures. On-line measurements of the temperature and independent tests with an atomic force microscope, performed on the Al cathode before and after current flow, demonstrated that the observed enhancement of the Raman signal was partly thermal and partly electromagnetic in origin, with clear evidence of cathode roughening induced by current flow. In contrast, analogous tests performed on P3OT-based OLEDs containing a composite Al + Ag cathode showed that the breakdown was related to electrode delamination.

PACS 78.60Fi; 78.30Jw; 85.60Jb

1 Introduction

Light-emitting diodes based on organic electroluminescent materials (OLEDs) have been actively studied since the late 1980s [1]. These devices offer big advantages with respect to their inorganic counterparts in terms of processability, cost reduction, color tunability and low voltage operation. Moreover, the development of OLEDs based on polymeric compounds, instead of small luminescent molecules, is expected to open the way towards the construction of flexible and inexpensive roll-up displays. Although very significant results have been obtained in the past ten years, the behaviour of polymer LEDs still requires in-depth investigation. In particular, new electroluminescent materials are currently being tested and the different mechanisms that limit device lifetime, both under storage and operating conditions, are widely investigated in the literature.

Up to now, many degradation and failure mechanisms have been identified [1–10]. In the first place, the interaction with water and oxygen produces a quenching of the emission and eventually the failure of devices. In order to impair this effect, experiments on OLEDs are currently performed under vacuum or inert atmosphere. However, photo-oxidative degradation can still take place, due to oxygen diffusion from indium-tin-oxide (ITO) anode into the active layer [1]. Solid-state morphology also plays a key role in determining the lifetime of a device [2–4]. Several authors observed that degradation and subsequent failure of OLEDs was accompanied by the formation of black spots, that were associated with local short-circuits or morphological, physical and chemical modifications of device structure. In some cases, black spots led to delamination of the structure and final detachment of the electrodes. A detailed analysis of the mechanism of black spot growth and of their nature is reported in the literature in both cases of polymer [5, 6] and small molecule [7–10] based electroluminescent devices.

In order to get a deeper understanding of the origin and evolution of the degradation processes, OLEDs have been investigated by using a large number of different techniques, such as microscopy (scanning and transmission electron microscopy, atomic force microscopy-AFM, scanning tunnelling microscopy, optical microscopy) [2–10], Auger electron spectroscopy [6, 10], secondary ion mass spectrometry [5], UV, and X-ray photoelectron spectroscopy in ultra-high vacuum [11], in situ infrared spectroscopy [12, 13], and microRaman spectroscopy performed on damaged areas after breakdown [14]. To the authors' knowledge, there are no reports in the literature on the use of Surface Enhanced Raman Scattering (SERS). SERS spectroscopy is extensively used to investigate the properties of molecules adsorbed on metals. It is well known that molecules, which are in close vicinity to properly roughened films or nanoparticles of silver, gold or, to a lesser extent, aluminum (currently used as the cathode in OLEDs), can undergo huge magnification of the Raman scattering that, in the case of silver, may be of the order of $\approx 10^6 \div 10^{14}$, and is dramatically dependent on the morphology of the enhancing metal surface [15]. In fact, when the ligand interacts with the metal surface, the Raman intensities undergo changes on the basis of the surface selection rules, which depend both on electromagnetic and chemical mechanisms, by enhancement of the local electric field at the metal surface and of the dynamic polarizability of the ligand, respectively. Moreover, the spectral positions of the SERS bands can present frequency-shifts with respect to the Raman spectrum of the bulk, by changes of the force constants. As a consequence, SERS appears to be a convenient tool for the characterization of the organic/metal interface in OLED

✉ Fax: +39-055-410-893, E-mail: e.giorgetti@ifac.cnr.it

devices. In particular, during OLED operation, enhancement factor, relative intensities and frequency-shifts of the Raman bands can exhibit variations associated with current flow. The aim of this paper is to propose SERS as a technique for on-line monitoring of OLEDs and, in particular, for efficient detection of several effects, such as heating, morphological changes at the organic film/cathode interface, formation of new chemical species or of chemical bonds between metal layer and active material [16], or simply degradation of the emitting molecules.

In order to assess the potential of SERS for OLED characterization, we performed some experiments on simple structures, based on a commercial and well-characterized active material: poly(3-octylthiophene) (P3OT) [17, 18]. Section 2 contains the details of OLED preparation and electric characterization, while Sect. 3 is devoted to the description of the Raman experiments performed with P3OT in different phases. Some AFM tests, reported in Sect. 3, were performed to independently check the SERS results.

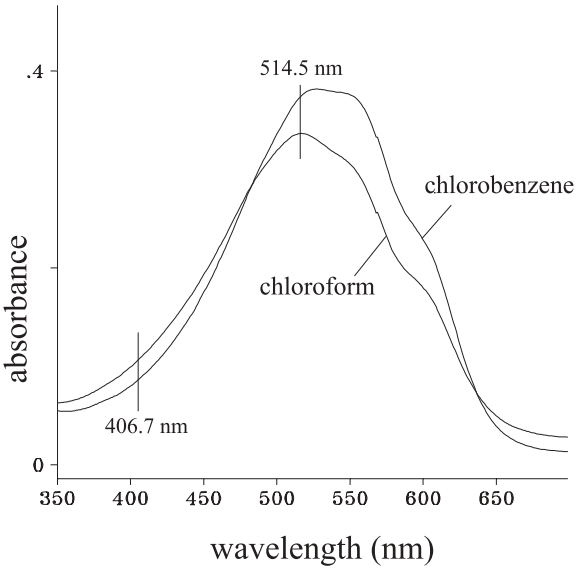

FIGURE 1 Electronic spectra of P3OT films obtained from chlorobenzene and chloroform solutions and spun on commercial microscope glass slides

2 OLED preparation

All the devices used in this study contained a single active layer made of regioregular commercial P3OT purchased from Aldrich. Indium-tin-oxide (ITO) was used as the anode, while the cathode was either a single Al layer or a mixture of Al and Ag. All the fabrication steps were performed under clean room conditions.

ITO coated substrates were purchased by Thin Film Devices. The ITO coating had nominal thickness and resistivity of 140 nm and $10^{-3}\ \Omega$ cm, respectively. Before deposition of the P3OT layer, ITO surfaces were patterned by photoresist-based lithography. Each sample contained four active regions and the typical dimensions of emitting areas were $4 \times 5\ \text{mm}^2$. After the patterning, ITO coated substrates were washed in trichloroethylene, acetone, 5% Decon mixture and finally rinsed in deionized water. All these operations were performed in an ultrasonic bath.

P3OT was dissolved in chlorobenzene and the films were obtained by spin coating of 10 g/l solutions filtered with 0.45 μm membranes. The thickness of the polymer layers was measured with a stylus profilometer and was, typically, of the order of 50 to 80 nm. Figure 1 shows the electronic spectra of P3OT films obtained from chloroform and chlorobenzene solutions. We preferred chlorobenzene to the currently used chloroform [19], because it permits higher and faster solubility and limits the recrystallization of films after the spin coating, which can be a severe problem for VP3OT [20]. We also observed that the use of chlorobenzene improves the quality of the deposition, particularly when it is performed after a moderate heating of substrate and solution, as well.

Immediately after the spin coating of P3OT, we fabricated top electrodes by electron gun evaporation. In general, we used aluminum electrodes with thickness of about 200 nm. However, we also prepared some samples containing a two-layer cathode made of Ag and Al. First, a 17 nm thick layer of Ag was thermally evaporated onto the polymer at a slow rate (≈ 0.2 Å/sec). The slow rate was aimed at producing a layer consisting mainly of silver islands and voids. Then, a 180 nm-thick Al layer was thermally evaporated onto silver at a rate of ≈ 10 Å/sec. This double deposition was chosen not only to enhance the SERS signal, due to the presence of silver nanoclusters, but also to simulate possible unwanted effects in those devices containing composite cathodes based on extremely thin layers of metals with a low work-function, such as Ca and Mg, and a thick cover layer of Ag [1].

All the devices were stored and tested under a vacuum of $\approx 10^{-2}$ Torr. Figure 2 shows a typical sample positioned within the vacuum chamber. When biased above ≈ 4 V, the device emits orange light and is clearly visible under standard room illumination conditions.

Current–voltage (I–V) characteristics of the OLEDs were recorded in constant voltage mode, by using a DC power supplier. Luminescence–voltage characteristics were measured with a calibrated silicon photodiode. The power efficiency of the devices, defined as

$$\eta = \frac{P_{\text{tot}}}{IV} \times 100, \tag{1}$$

was obtained from the measured optical power P by calculating the total emitted power P_{tot} in the hypothesis of a Lambertian point source and by taking into account the distance

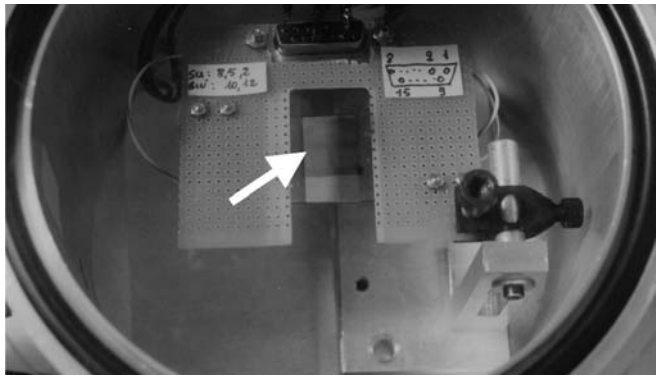

FIGURE 2 One of our samples positioned inside the vacuum chamber used for all the experiments. The *arrow* indicates one of the four active areas

between emitting area and window of the vacuum chamber and the reflectivity of the window.

Figure 3 shows the I–V characteristics of four of our ITO/P3OT/Al samples and, in one case (crosses), of an ITO/P3OT/Ag+Al sample. The optical power-voltage characteristic of one of the ITO/P3OT/Al samples is also reported in the inset of Fig. 3. The corresponding efficiency evaluated in the peak of the curve was $\eta = 4 \times 10^{-4}\, V\%$. As shown in Fig. 3, I–V characteristics of ITO/P3OT/Al samples exhibit a considerable repeatability and diode operation was very stable in terms of current flow and emitted power for voltages up to 8 V, corresponding to a dissipated electrical power of the order of 300 mW. However, the emitted optical power decayed abruptly above 8 V (see the inset of Fig. 3b) and some current instability was observed. Device breakdown occurred at bias voltages of around 15 V, corresponding to a dissipated power of ≈ 2 W. Typical breakdown values for ITO/P3OT/Ag + Al samples were lower (10 V bias and 600 mW dissipated power), apparently due to the presence of Ag that, although advantageous for SERS experiments, quenches the efficiency of the diodes and anticipates the breakdown [20].

In general, we did not obtain any evidence of the formation of black spots, even under on-line optical microscope inspection (up to 40X magnification). Only in the case of one aged ITO/P3OT/Al sample, did we observe black spots and bubbles. After a three-month-long storage time under 10^{-2} Torr vacuum, the sample was operated for several hours with repeated ON/OFF cycles. Its behavior, both in terms of I–V characteristics and of surface illumination, was the same as that observed for fresh samples. However, during the operating cycle described by the sequence of pictures of Fig. 4a–e,

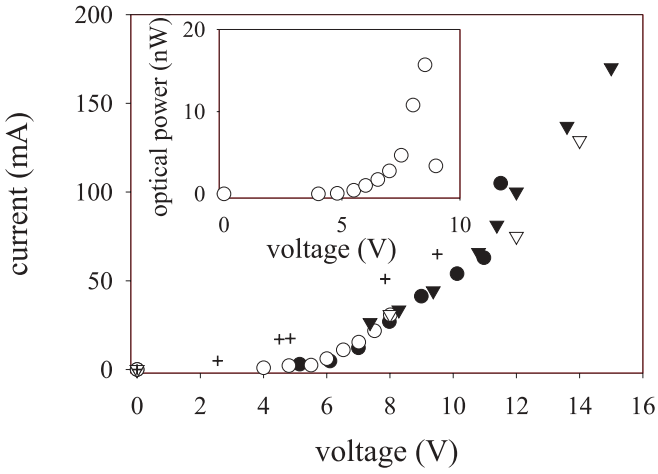

FIGURE 3 I–V characteristics of four ITO/P3OT/Al devices and of one ITO/P3OT/Ag+Al device (*crosses*). The *inset* shows optical power-voltage characteristics of one ITO/P3OT/Al sample

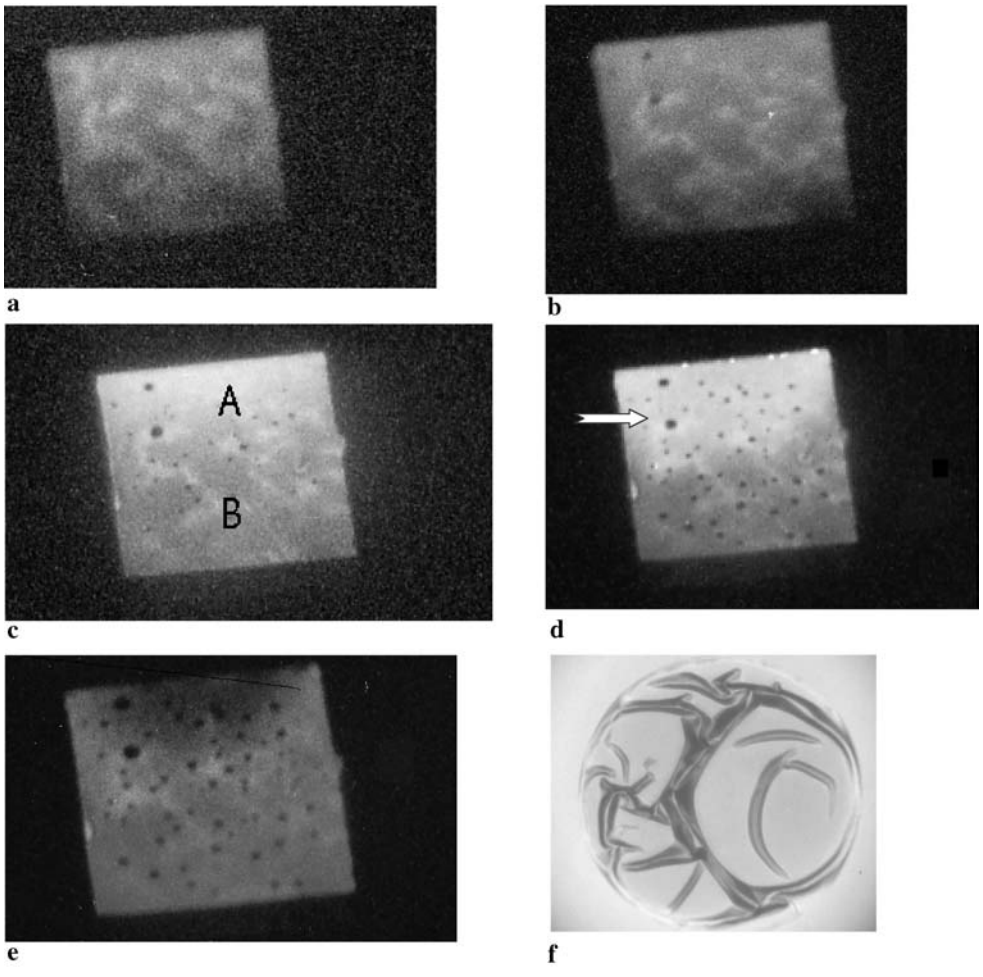

FIGURE 4 Operation of an aged ITO/P3OT/Al device. **a** 7 V bias after tens of ON/OFF cycles: the active area is partially illuminated and there is no evidence of black spots; **b** 7 V bias at the beginning of the last cycle before breakdown: the active area is partially illuminated and three black spots are well visible in the brightest region; **c** 8 V bias: the emission intensity of the initially bright area (A) has grown, the initially dark area (B) has started to emit and the black spots have diffused throughout the emissive region; **d** after several minutes operation at 9.5 V bias: some sparks start to appear at the edge of region A; **e** after several minutes operation at 13.5 V bias: area A has switched OFF, while area B is still emitting; **f** microscope view of the bubble indicated by the arrow in **d**, taken with 200X magnification

we observed the formation of several black spots. Eventually, after some more minutes of operation at 13.5 V (Fig. 4e), the OLED broke down and bubbles were clearly visible to the naked eye. Their position corresponded to the black spots observed during OLED emission. Figure 4f shows a microscope picture of the bubble indicated by the arrow in Fig. 4d.

Apart from the presence of black spots and bubbles, the sequence of Fig. 4a–e also represents the typical evolution of ITO/P3OT/Al samples, in terms of surface illumination and uniformity of the emission. In particular, when OLEDs are switched ON, some macroscopic regions of the surface may appear dark (Fig. 4a,b). The morphology of bright and dark areas does not change with repeated switching ON and OFF of the devices and seems to be related with the uniformity of the active layers. Indeed, it is well known that OLED efficiency is strongly dependent on the value of the electric field (more than bias voltage) and, consequently, on the thickness of the active layer [21]. Above 8 V, when device instabilities and power decay begin, the initially bright areas (marked with A in Fig. 4c) gradually loose permanently their permanent efficiency, while the initially dark areas (marked with B in Fig. 4c) switch ON (Fig. 4e).

3 Raman experiments

Raman spectra were recorded using the 514.5 and 457.9 nm lines of an Ar^+ laser or the 647.1 and the 406.7 nm lines of a Kr^+ laser. Samples were irradiated by using $40 \div 150$ mW laser power and the laser beam was defocussed to impair thermal effects or quenching of the Raman signal. Power density measurements were performed with a power meter (model 362; Scientech) and gave an accuracy of $\sim 5\%$ in the 300–1000 nm spectral range. The scattered light was collected at 90° with respect to the plane of the samples and detected by a Jobin-Yvon HG2S monochromator equipped with a cooled RCA-C31034A photomultiplier and a data acquisition facility. Spectra were usually registered on-line, during OLED operation, and at different bias voltages. The samples were continuously kept under 10^{-2} Torr vacuum, by means of a rotative pump (Fig. 2).

Due to the well-known SERS efficiency of silver nanoclusters, we performed the first Raman tests with OLED samples having Ag + Al cathodes. We started with the 514.5 nm exciting line that, as shown by the electronic spectra of Fig. 1, induces a resonant Raman effect on P3OT. Figure 5 shows the Raman spectra of an ITO/P3OT/Al + Ag sample, recorded at different bias voltages and, for comparison, the spectrum of a powder sample of P3OT. In this case, due to the resonance, the Raman spectra were mainly produced by the bulk response of the polymeric layer and the SERS effect at the polymer/metal interface was masked. No appreciable difference was observed among spectra registered before switching ON ($V = 0$) and during OLED operation, apart from an increase of the background signal, due to the enhanced luminescence of the device, associated with current flow.

Figure 6 shows the Raman spectra of the same device of Fig. 5 and of a powder sample, registered with the 406.7 nm exciting line. In this case, the resonant contribution was considerably reduced (Fig. 1) and the Raman signal of the OLED was mainly associated with a SERS effect. All the main bands

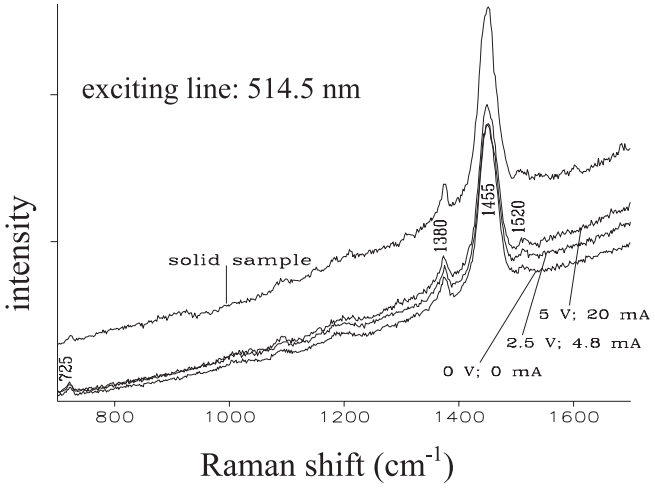

FIGURE 5 Raman spectra of an ITO/P3OT/Ag+Al sample recorded at different bias voltages. The spectrum of a P3OT powder sample is also reported for comparison. Exciting wavelength $\lambda = 514.5$ nm, laser power 40 mW

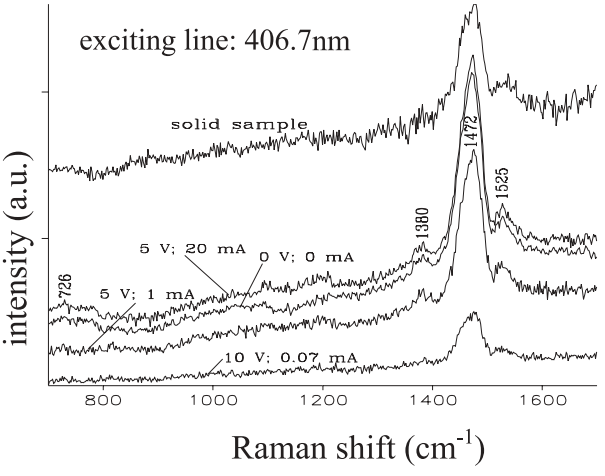

FIGURE 6 SERS spectra of the same device of Fig. 5 recorded at different bias voltages. The spectrum of a P3OT powder sample is also reported for comparison. Exciting wavelength $\lambda = 406.7$ nm, laser power 40 mW

occurring at $I = 0$ are attributed to the vibrations of the thiophene ring [22, 23]. In particular, the bands at 1525 cm^{-1} and 1472 cm^{-1} are associated with antisymmetric and symmetric C = C stretching , respectively. The band at 1380 cm^{-1} is associated with the C − C ring stretching, while the band at 726 cm^{-1} is associated with C − S − C bending. In general, the band at 1472 cm^{-1} is known as the amplitude mode.

The most intense band of the spectrum of Fig. 6 (1472 cm^{-1}) was considerably shifted (1455 → 1472 cm^{-1}) with respect to the spectra of Fig. 5. A minor shift was also detected for the band at 1525 cm^{-1} (1520 → 1525 cm^{-1}). A similar Raman dispersion, which at a first glance could be due to a chemical adsorption of the polymer on the metal layer, was already described for the case of poly(3-decylthiophene) [24] and for P3OT films on dielectric substrates [22]. The dispersion observed in [22] regarded only the C = C symmetric ring stretching band and was attributed to the coexistence of polymeric chains having different conjugation lengths and, hence, different Raman resonances. Indeed, by using a standard deconvolution procedure (Fig. 7), we

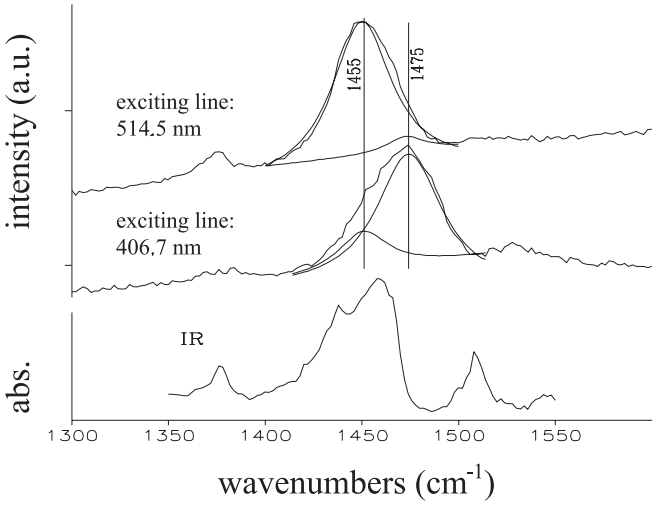

FIGURE 7 Deconvolution of the C = C symmetric stretching bands of Figs. 5, 6 and IR spectrum of P3OT in KBr pellets

found that the amplitude mode of Fig. 6 exhibits a shoulder at 1455 cm^{-1}, corresponding to the band observed with the green exciting line. At the same time, the band observed at 1455 cm^{-1} in the spectra of Fig. 5 exhibits a shoulder at 1475 cm^{-1}. To clarify this point, we examined the IR spectrum of P3OT in a KBr pellet. This spectrum, shown in Fig. 7, permits observation of the C = C stretching in absence of the Raman resonance, and consists of a wide band from 1440 cm^{-1} to 1470 cm^{-1}, with a maximum at 1455 cm^{-1}. Moreover, we also observed that the dispersion of the Raman bands associated with C = C stretching not only occurs in the spectra of P3OT powders and films, but also in samples consisting of P3OT in Ag colloids. For this purpose, stable silver sols were prepared by reduction of $AgNO_3$ (Aldrich, purity 99.998%) with excess $NaBH_4$ (Aldrich, purity 99%) [25] and aged a week to prevent the formation of reduction products [26]. The typical pH value of the aqueous suspension was ≈ 9. SERS spectra of P3OT in Ag hydrosol are shown in Fig. 8: also in this case, Raman bands associated with C = C stretching move to higher frequencies with decreasing exciting wavelength. In light of all these observations, we could definitely exclude the chemisorption of P3OT on the Ag + Al layer and attribute the SERS signal of Fig. 6 to a purely electromagnetic effect and the dispersion of the Raman signal to the existence of a wide distribution of conjugation lengths that resonate with different exciting laser lines.

Figure 6 also shows SERS spectra recorded during OLED operation. At first, no significant changes were observed between 0 and 5 V bias (spectra registered before switch ON and at $I = 20$ mA were identical). However, after several minutes operation at 5 V (corresponding to a dissipated power of only 100 mW) and some ON/OFF cycles, the OLED appeared to be seriously damaged. The same bias voltage of 5 V produced a current flow of only 1 mA, although the SERS spectrum appeared unchanged. An attempt to increase the current flow by biasing the device up to 10 V produced a fast decrease of current flow (down to 0.07 mA) and a sudden decay of the SERS signal, with no change in the spectral position of the main Raman bands. This behaviour is consistent with a detachment of the active layer from the cathode, probably due to a huge field intensification and consequent local increase of temperature at silver sites.

SERS tests at 406.7 nm were repeated with Ag-free samples. In this case, a reduced Raman signal was expected, due to the lower SERS activity of Al. However, the absence of Ag in the OLED structure improved both efficiency and stability of the devices and moved breakdown threshold towards higher levels of bias voltage. The results of Raman tests on a ITO/P3OT/Al sample are reported in Fig. 9. In order to better identify the positions of the bands, all spectra have undergone the same smoothing procedure by the Savitsky–Golay method. In this case, the SERS effect could not be attributed entirely to an electromagnetic mechanism, because the initial ($V = 0$) position of the amplitude mode was down-shifted with respect to that of P3OT powders (see Figs. 6 and 7). This provides indication of a weak interaction between Al and polymer at the interface. SERS spectra of Fig. 9 were recorded at different bias voltages. For moderate bias voltage (between 0 and 8 V), OLED operation was stable, although with non-uniform surface illumination (Fig. 4). No appreciable changes of SERS spectra were observed within this voltage range, apart from a minor growth of the background signal due to the

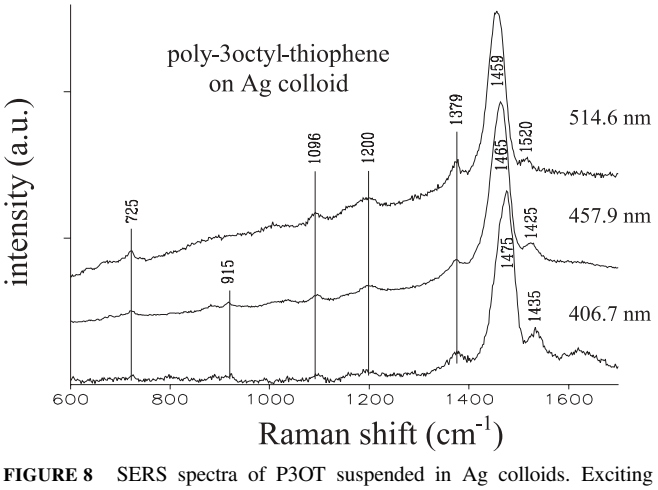

FIGURE 8 SERS spectra of P3OT suspended in Ag colloids. Exciting wavelengths λ =: 406.7, 457.9 and 514.5 nm

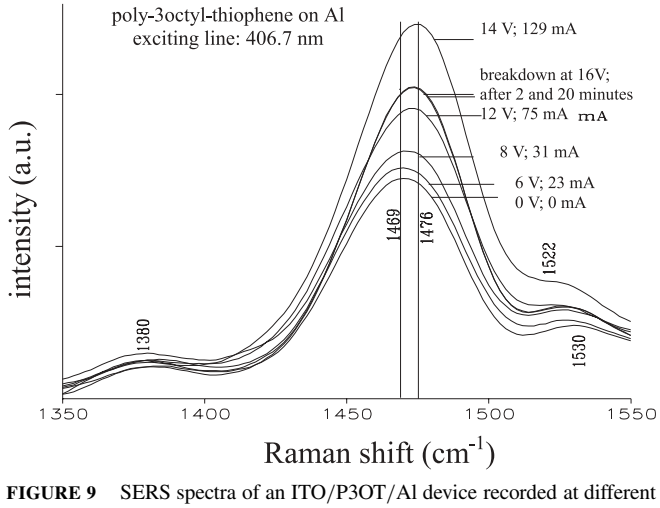

FIGURE 9 SERS spectra of an ITO/P3OT/Al device recorded at different bias voltages. Exciting wavelength λ = 406.7 nm, laser power 150 mW

voltage-induced increase of the fluorescence level. However, for a bias voltage larger than 8 V, we observed that the Raman band at 1469 cm^{-1} grew considerably and its centre frequency moved toward larger values (1469 $cm^{-1} \rightarrow$ 1476 cm^{-1}), that is, towards the spectral position pertaining to P3OT powders, that was reached at 14 V bias. At the same time, device sites that were very efficient at low bias started to loose their brightness, while other areas became more efficient. Eventually, at 16 V bias voltage, OLED breakdown occurred and the intensity of the Raman band decayed, but without recovering its initial value. The difficult peel-off of the cathode with adhesive tape and the stable and large SERS signal after the breakdown suggested that, in this case, cathode delamination did not take place.

The Raman enhancement reported in Fig. 9 could be interpreted in terms of an electric field-induced increase of cathode roughness [27] that in turn, produced an avalanche growth of the electric field and so on, until OLED broke down, first in the areas that were more emissive at low bias. However, the same enhancement and the up-shift of the Raman amplitude mode could also be explained in terms of a heating of the polymer film, according to the experiments reported in [22] for films and in [28] for powders of P3OT.

We monitored on-line the operating temperature of some ITO/P3OT/Al samples, in order to assess the thermal contribution to our SERS results. For this purpose, we placed a temperature sensor on the emitting areas. We observed that for bias voltages up to 8 V, device temperature kept around 40–45 °C. Temperature rapidly grew up to 95 °C for bias voltages around 12–13 V and was around 100 °C at breakdown. At first glance, this temperature increase could explain the up-shift of the amplitude mode. Indeed, in [28], where Raman spectra of P3OT powders were excited at 1064 nm, a negligible shift of the Raman amplitude mode was observed for temperatures below 40 °C, while a total 8 cm^{-1} up-shift was observed by heating up to 127 °C. This value was interpreted as an indication of the poor dependence on temperature of the backbone conformation. However, in our case, the permanent nature of the up-shift of the Raman mode (no down-shift was detected after breakdown and consequent cooling) and the different structure of the sample under observation, consisting of a film in contact with a metal layer, suggested that the thermal contribution to the up-shift, if any, was negligible with respect to the chemical interaction between polymer chains and aluminum. In contrast, the observed temperature increase of operating samples can provide a contribution to the Raman enhancement. Indeed, Raman spectra of P3OT films on quartz excited at 406.7 nm are reported in ref. [22], where the intensity of the amplitude mode increases continuously from room temperature up to 97 °C and than decays above this temperature. This effect was interpreted in terms of a reversible thermochromic transition of the polymer [22]. In our case, the persistence of the Raman enhancement even after 2 and 20 minutes from breakdown, led us to conclude that the most liable mechanism responsible for it is the simultaneous occurrence of roughness and temperature effects.

In light of the previous considerations, we performed AFM tests in order to check the morphology of ITO/P3OT/Al devices. Topography was measured ex situ in a dry nitrogen atmosphere, using a Molecular Imaging AFM (PicoSPM, Molecular Imaging) operating in contact mode, with a commercial Si_3N_4 cantilever (Nanosensors, Wetzlar-Blankenfeld). The quality of the samples, characterized by non-filtered 512 × 512 pixel images was checked through the root mean square roughness parameter (RMS), provided by the AFM software. RMS roughness was calculated via the

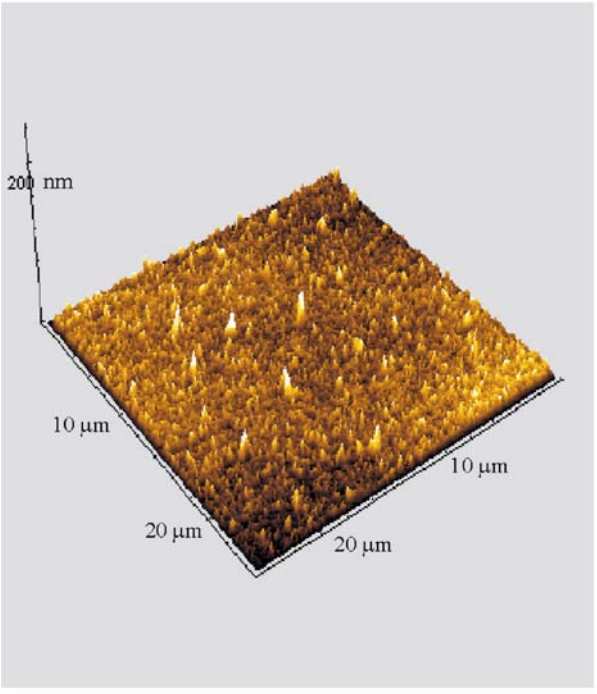

a

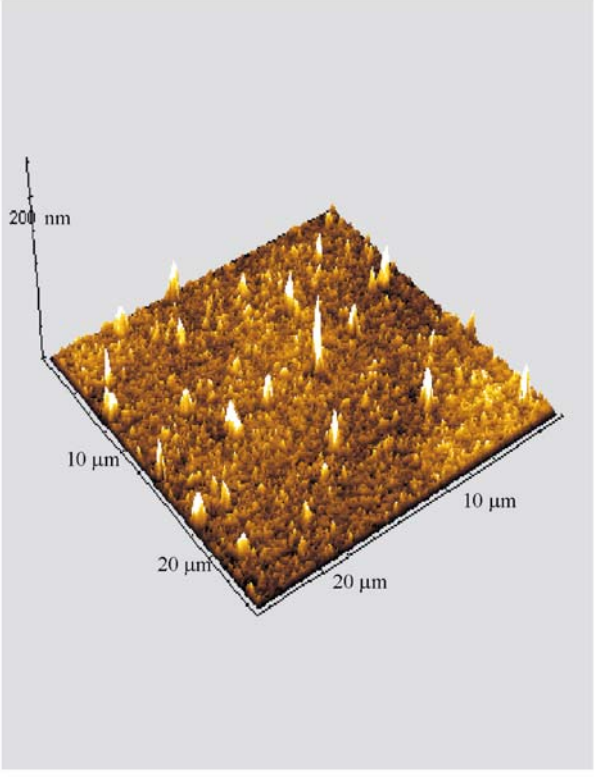

b

FIGURE 10 AFM picture of Al cathode before (**a**) and after (**b**) current flow

standard formula:

$$\mathrm{RMS}^2 = (1/N)\,\Sigma_{ij}[h_{ij} - h]^2\,. \quad (2)$$

Here, N is the number of pixels in the image, h_{ij} is the local height at pixel ij, and h is the mean height.

ITO electrodes were inspected by AFM before and after OLED breakdown. For this purpose, the Al layer was peeled off by adhesive tape and the polymer film was washed away in warm chloroform. The ITO surface appeared very smooth, with an RMS roughness of the order of 2 nm. In contrast, Al electrodes exhibited a very different behavior. Figure 10a shows the morphology of the Al cathode before current flow. In this case, the RMS roughness evaluated on a $10 \times 10\ \mu\mathrm{m}^2$ area, was 7.4 nm with peak-valley fluctuations of 42 nm and an average cluster radius of 138 nm. Figure 10b shows an image of the same electrode after current flow: we detected a clear increase of surface roughness corresponding to a value of 9.1 nm RMS, with peak-valley fluctuations of 72 nm and an average cluster radius of 178 nm. It is reasonable to attribute the permanent part of the growth of the SERS signal with current flow reported in Fig. 9 to this roughening of the Al layer and to exclude significant contributions of the ITO electrode in the process.

SERS experiments were also performed on the sample of Fig. 4 after breakdown, in order to investigate the origin of the bubbles. However, we did not detect any difference among the SERS spectra registered in different regions of the sample and on similar samples not exhibiting bubbles after breakdown. This result indicated that, on average, there were no chemical modifications of the emissive layer, at least in the vicinity of the cathode. A possible explanation of bubble formation in the aged sample is in the oxygen diffusion within the active layer, with subsequent outgassing activated by temperature increase during OLED operation.

4 Conclusions

In this paper, we presented a SERS study of OLEDs based on the commercial polymer P3OT. Although a detailed investigation of Raman and SERS response of P3OT on roughened gold electrodes and Ag colloids was recently presented in [23], to the authors' knowledge, SERS had never been adopted before as an on-line probe to monitor OLED operation.

We performed most experiments with ITO/P3OT/Al devices. However, we also characterized some devices containing Ag + Al cathodes. Ag was primarily added to the Al cathode in order to enhance the SERS gain. Although the presence of Ag had a negative influence on device performance, both in terms of efficiency and durability, however, a check of the behavior of Ag-containing devices may be of general interest. In fact, Ag nanoclusters can form at polymer/cathode interfaces in structures that contain composite cathodes based on ultra-thin Ca or Mg films acting as electron injecting electrodes, with Ag as a cover protective layer. In these cases, SERS tests can represent a powerful tool to probe the structure of the co-evaporated cathode and, in particular, unwanted contact between silver and active material.

Generally speaking, our experiments show that SERS tests can be of valuable help in the characterization of OLEDs: a) to get information about the distribution of polymer chain length (the Raman modes related with C = C stretching shift with exciting wavelength); b) to probe the existence of chemisorption at polymer/metal interface (from the differences among SERS spectra and spectra registered from powders or films deposited on dielectric substrates); c) to observe cathode delamination from the active layer (from the decay of the Raman signal with OLED bias voltage); d) to monitor electric field induced cathode roughening and to detect anomalous heating of the polymer layer (from Raman enhancement and/or shift of the C = C stretching modes).

ACKNOWLEDGEMENTS This research was partially supported by the Italian Project on Nanotechnologies (legge 95/95) and by the joint project between Italian CNR and Mexican CONACYT on "Synthesis and characterization of novel conjugated molecules for optical applications". The authors are indebted to Alberto Bolognesi (ISMAC-CNR, Milano, Italy) for stimulating discussions.

REFERENCES

1 C.W. Tang, S.A. VanSlyke: Appl. Phys. Lett. **51**, 913 (1987); J.H. Burroughes, D.D.C. Bradley, A.R. Brown, R.N. Marks, K. Mackey, R.H. Friend, P.L. Burns, A.B. Holmes: Nature **347**, 539 (1990); U. Mitschke, P. Bäuerle: J. Mater. Chem. **10**, 1471 (2000)
2 E. Ettedgui, G.T. Davis, B. Hu, F.E. Karasz: Synth. Met. **90**, 73 (1997)
3 H. Razafitrimo, Y Gao, W.A. Feld, B.R. Hsie: Synth. Met. **79**, 103 (1996)
4 J.R. Rasmusson, P. Bröms, J. Birgerson, R. Erlandson, W.R. Salaneck: Synth. Met. **79**, 75 (1996)
5 L. Ke, S. Chua, K. Zhang, N. Yakovlev: Appl. Phys. Lett. **80**, 2195 (2002)
6 B.H. Cumpston, K. F Jensen: Appl. Phys. Lett. **69**, 3941 (1996)
7 J. McElvain, H. Antoniadis, M.R. Hueschen, J.N. Miller, D.M. Roitman, J.R. Sheats, R.L. Moon: J. Appl. Phys. **80**, 6002 (1996)
8 Y. Liew, H. Aziz, N. Hu, H. Sze-On Chan, G. Xu, Z. Popovic: Appl. Phys. Lett. **77**, 2650 (2000)
9 P.E. Burrows, V. Bulovic, S.R. Forrest, L.S. Sapochak, D.M. McCarty, M.E. Thompson: Appl. Phys. Lett. **65**, 2922 (1994)
10 M. Kawaharada, M. Ooishi, T. Saito, E. Hasegawa: Synth. Met. **91**, 113 (1997)
11 W.R. Salaneck, J.L. Bredas: Adv. Mater. **8**, 48 (1996)
12 J.C. Scott, J.H. Kaufman, P.J. Brock, R. DiPietro, J. Salem, J.A. Goitia: J. Appl. Phys. **79**(5), 2745 (1996)
13 B.H. Cumpston, I.D. Parker, K.F. Jensen: J. Appl. Phys. **81**(8), 3716 (1997)
14 Ji-Seon Kim, Peter K.H. Ho, C.E. Mirphy, N. Baynes, R.H. Friend: Adv. Mater. **14**(3), 206 (2002)
15 G.C. Schatz, R.P. Van Duyne: *Electromagnetic mechanism of surface-enhanced spectroscopy*, In: Handbook of Vibrational Spectroscopy, ed. by J.M. Chalmers, P.R. Griffiths, Wiley (2002) p. 759
16 W.E. Doering, S. Nie: J. Phys. Chem. B **106**, 311 (2002)
17 D. Braun, G. Gustafsson, D. McBranch, A.J. Heeger: J. Appl. Phys. **72**, 564 (1992)
18 M. Theander, O. Inganäs, W. Mammo, T. Olinga, M. Svensson, M.R. Andersson: J. Phys. Chem. B **103**, 7771 (1999)
19 G. Wang, C. Yuan, H. Wu, Y. Wei: J. Appl. Phys. **78**, 2679 (1995)
20 F. Garten, J. Vrijmoeth, A.R. Schlatman, R.E. Gill, T.M. Klapwijk, G. Hadziioannou: Synth. Met. **76**, 85 (1996)
21 P.E. Burrows, S.R. Forrest: Appl. Phys. Lett. **64**, 2285 (1994)
22 T. Danno, J. Kurti, H. Kuzmany: Phys. Rev. B **43**, 4809 (1991)
23 E.A. Bazzaoui, M. Bazzaoui, J. Aubard, J.L. Lomas, N. Falidj, G. Levi: Synth. Met. **123**, 299 (2001)
24 G. Louarn, M. Trznadel, J.P. Buisson, J. Laska, A. Pron, M. Lapkowski, S. Lefrant: J. Phys. Chem. **100**, 12532 (1996)
25 J.A. Creighton, C.G. Blatchford, M.G. Albrecht: J. Chem. Soc. Faraday Trans. II **75**, 790 (1979)
26 M. Muniz-Miranda, N. Neto, G. Sbrana: J. Mol. Struct. **174**, 351 (1988)
27 R.K. Kasim, Y. Cheng, M. Pomerantz, R.L. Elsenbaumer: Synth. Met. **85**, 1213 (1997)
28 A. Bolognesi, W. Porzio, A. Provatoli, C. Botta, A. Comotti, P. Sozzani, R. Simonutti: Macromol. Chem. Phys. **202**, 2586 (2001)